Efficient photocatalytic aerobic oxidation of bisphenol A via gas-liquid-solid triphase interfaces

Pu Wang [a, b], Jiaqi Zhao [a, b], Run Shi [a, **], Xuerui Zhang [a, b], Xiangdong Guo [b, c], Qing Dai [b, c], Tierui Zhang [a, b, *]

[a] Key Laboratory of Photochemical Conversion and Optoelectronic Materials, Technical Institute of Physics and Chemistry, Chinese Academy of Sciences, Beijing 100190, China
[b] Center of Materials Science and Optoelectronics Engineering, University of Chinese Academy of Sciences, Beijing 100049, China
[c] CAS Key Laboratory of Nanophotonic Materials and Devices, CAS Key Laboratory of Standardization and Measurement for Nanotechnology, CAS Center for Excellence in Nanoscience, National Center for Nanoscience and Technology, Beijing 100190, China

ARTICLE INFO

Keywords:
Triphase system
Photocatalysis
Oxygen transport
Au/TiO_2

ABSTRACT

As a promising environmental treatment technology, photocatalysis has been investigated for decades and even tentatively practiced in actual large-scale applications. However, most researches focus on photocatalytic kinetics (excitation, charge transfer, and surface reaction) but ignore the significant impact of oxygen interfacial mass transfer for photocatalytic aerobic oxidation in aqueous media. Here, we use finite element simulation to demonstrate that during photocatalysis, the remained local oxygen concentration for photocatalysts at a gas-liquid-solid triphase interface is much higher than that dispersed in a bulk liquid phase. Photocatalyst consisting of Au/TiO_2 nanoparticles supported at triphase interface shows a non-diffusion limited charge separation for oxygen photoactivation, therefore achieving a photodegradation efficiency of about 85% toward bisphenol A. Furthermore, we develop a flowing triphase photocatalytic system that exhibits a tunable one-way photodegradation efficiency from 10% to 60% and a photostability for up to 50 h of continuous irradiation, further demonstrating the potential for large-scale applications.

1. Introduction

Environmental problems, especially water pollution, are significant issues closely related to human survival and development that urgently need to be resolved on a global scale [1,2]. Bisphenol A [BPA, 2,2-bis(4-hydroxyphenyl)propane], a primary chemical raw material widely used in the production of epoxy resins, polycarbonate plastics and leather, is one of the most common endocrine-disrupting substances that can interfere with the human endocrine system [3]. BPA is one antioxidant that is non-biodegradable and highly resistant to chemical degradation [3,4], making it difficult for conventional organic wastewater treatment methods to efficiently remove BPA in water.

Semiconductor-based photocatalytic aerobic oxidation [5–7] is a promising water treatment technology to use solar energy for water remediation [8–10]. TiO_2 is one of the most investigated photocatalysts featured by its good activity, non-toxicity, and chemical stability [11,12]. The modification strategy of loading noble metals as cocatalysts can promote the migration of carriers and then waken the charge recombination over TiO_2. Especially for Au/TiO_2, the Fermi level of Au nanoparticles is significantly lower than the conduction band of TiO_2 [13,14], so electrons excited to the conduction band can spontaneously migrate to the Au surface, hence converting oxygen into reactive oxygen species (ROS), such as $\cdot O_2^-$ and $\cdot OH$, that can directly participate in the pollutant oxidation reaction. This aerobic oxidation process shows unique advantages in mineralizing chemically stable organic pollutants (such as phenol and other aromatic compounds) into inorganic carbons [15–17].

The mass transfer process that determines the local concentration of reactants at the reaction interface also has considerable impacts on the performance of heterogeneous catalysis [18]. In conventional liquid-solid diphase photocatalytic systems, where photocatalytic nanomaterials are dispersed in bulk aqueous media,

* Corresponding author.
** Corresponding author.
E-mail addresses: shirun@mail.ipc.ac.cn (R. Shi), tierui@mail.ipc.ac.cn (T. Zhang).

ROS can only be generated from dissolved oxygen that diffuses very slowly in the water phase. The mass transfer of oxygen molecules on the surface of photocatalysts might be an insurmountable obstacle to increase the overall photocatalytic reaction rate [19]. The construction of gas-liquid-solid triphase interfaces can alter the interfacial mass transfer behavior of the gas reactant molecules and directly affect the kinetics of the catalytic reaction [20,21]. Theoretically, triphase photocatalysis realizes the effective contact of oxygen, water, and photocatalysts, resulting in the rapid supply of oxygen from the gas phase instead of dissolved oxygen molecules from the water phase [22]. Feng et al. [18] developed a triphase photocatalytic system in which the photocatalytic reaction can proceed at the gas-liquid-solid three-phase interface, showing a high photodegradation efficiency toward salicylic acid. However, the local oxygen concentration on the surface of photocatalysts during photocatalytic reactions and its relationship toward charge separation and photodegradation efficiencies has yet to be well understood. Besides, previous triphase photocatalytic oxidation reactions mainly focused on dye molecules, the activity in dealing with refractory organic pollutants such as BPA remains to be further investigated.

Herein, we investigate the photocatalytic aerobic oxidation reaction for BPA degradation by constructing a gas-liquid-solid triphase system, in which hydrophilic Au/TiO_2 nanoparticles are supported at the air-water boundary. Through finite element simulations, we find that during photocatalysis, the triphase interface can maintain a relatively high local oxygen concentration. In contrast, the dissolved oxygen in the diphase system where the catalyst is immersed in the bulk liquid phase will be quickly run out as the photocatalytic reaction progresses. The triphase photocatalytic system has a much higher BPA degradation percentage up to 85%, while BPA in the diphase system can hardly be degraded mainly because of the interfacial oxygen mass transfer limitation. In addition, we have obtained up to 50 h of photocatalytic stability in a flowing triphase photocatalytic system, showing its potential for large-scale practical applications.

2. Materials and methods

2.1. Chemicals and materials

TiO_2 (P25) was purchased from Degussa AG. $HAuCl_4$ and ethanol were obtained from Aladdin. $NaBH_4$ was purchased from Guangdong Guanghua Chemical Factory Co., Ltd. BPA, 4,4′-Sulfonyldiphenol (BPS) and 4,4′-(Hexafluoroisopropylidene)diphenol (BPAF) were acquired from Innochem. All chemicals were used without further purification. Microporous carbon gas diffusion layers (GDLs) were purchased from Germany Freudenberg (H14C9). Doubly distilled water was used in all experiments.

2.2. Photocatalyst preparation

Preparation of photocatalysts Au/TiO_2: Au nanoparticles were loaded on TiO_2 photocatalysts via a $NaBH_4$ reduction method. The precursor was $HAuCl_4 \cdot 4H_2O$. In more detail, 1.0 g TiO_2 was dispersed into 100 mL water, followed by ultrasonication for 30 min. Then 200 μL aqueous $HAuCl_4$ solution (50 mg/L for Au) was added to the suspension by ultrasonication for 5 min. Then 10 mL aqueous $NaBH_4$ solution (0.5 mg/mL) was added dropwise to the suspension under stirring, with the color of the suspension gradually turning purple. After further stirring for 2 h, the samples were centrifuged and washed with water three times, and then vacuum freeze-dried for 24 h.

Preparation of Au/TiO_2 immobilized GDL: Au/TiO_2 distributed in ethanol (0.5 mg/mL) was sonicated for at least 30 min to form a uniform dispersion. Then, Au/TiO_2 was immobilized onto the surface of GDL substrate by dripping a 5 mL suspension onto the surface of GDL and dried under infrared light for 1 h to form a photocatalysts layer with an area of 3.5 × 3.5 cm^2, receiving an Au/TiO_2 immobilized GDL with a loading amount 0.2 mg/cm^2. For the Au/TiO_2 immobilized GDL used in the flowing test, the area of GDL was 5.0 × 5.0 cm^2, the corresponding dispersion volume was 10 mL, and other operations were the same. For diphase system preparation, the Au/TiO_2 was immobilized onto a quartz plate substrate using the same method.

2.3. Characterization

Morphologies of the samples were observed by scanning electron microscopy (SEM, Hitachi, S4800, Japan) and transmission electron microscope (TEM, JEM, 2100F, Japan). The structure and crystallization of the particles were examined by X-ray diffraction (Bruker AXSD8 Advance, Germany) equipped with a Cu Kα radiation source (λ = 1.5405 Å) operating at 40 kV. X-ray photoelectron spectroscopy (XPS) data were obtained on ESCALAB 250Xi (Thermo Fisher Scientific, USA) using monochromatic Al-Kα radiation (hν = 1486.6 eV) as the excitation source. Binding energies were calibrated by the C1s peak at 284.8 eV of neutral carbon. The diffuse reflection spectra of the as-prepared photocatalyst powders were recorded on Cary 7000 (Agilent) spectrometer with an integrating sphere attachment. A contact angle system (OCA20, Dataphysics, Germany) was used to measure the contact angles, with the probe liquid being a 2.0 μL droplet of water. The result was average values obtained from more than three different positions. Photocatalytic performance was measured by a ultraviolet-visible (UV−Vis) spectrophotometer (Hitachi U-3900). Oxygen radicals were measured by electron paramagnetic resonance spectroscopy (Bruker E500, Germany). The total organic carbon (TOC) of samples was measured by a TOC analyzer (Analytik Jena Multi N/C TOC/TN, Germany).

2.4. Photoelectrochemical measurement

The photoelectrochemical measurements were carried out on an electrochemical workstation (CHI 660e) using a homemade microfluidic reactor equipped with a quartz window as the photoelectrochemical cell. 1 M Na_2SO_4 aqueous solution was used as an electrolyte. Ag/AgCl and Pt wire were used as reference and counter electrodes, respectively. The working electrodes were prepared by dripping 400 μL of Au/TiO_2 dispersion (0.5 mg/mL) onto the GDL to form an area of 1 cm^2. For the triphase photocurrent test, the Au/TiO_2-immobilized GDL was directly used as the working electrode. For the diphase photocurrent test, the GDL of the working electrode was uniformly coated with vacuum silicone grease to diminish gas diffusion from the gas phase. The photocurrent tests were carried out at a potential of −0.211 V vs. Ag/AgCl (0.4 V vs. RHE) with chopped irradiation every 30 s.

2.5. Photocatalytic measurements

A 365 nm LED lamp (PLS-LED100C, PerfectLight, China) equipped with a λ < 400 nm filter (Xujiang Electromechanical Plant, Nanjing, China) was used as the light source. For the tests in a batch reactor, the as-prepared Au/TiO_2 immobilized GDL was placed onto the top of the liquid surface for the triphase system, and the as-prepared Au/TiO_2 immobilized quartz plate was placed into the liquid phase for the diphase system. Before light irradiation, the reactor was placed in the dark for 30 min to establish an adsorption equilibrium. The photocatalytic aerobic oxidation reaction time was 120 min, during which approximately 0.5 mL solution was

withdrawn with a pipette at every 20 min intervals. For the test in a flow reactor, a quartz beaker containing 10 mL BPA solution and a homemade flow cell was used as the photo-reactor. The as-prepared Au/TiO_2 immobilized GDL was fixed between the aluminum alloy bracket and the serpentine liquid flow path with the catalyst layer on the side close to the liquid. At intervals, the outlet solution was collected for further testing. Afterward, the concentration of BPA was detected by the intensity of the characteristic absorption peak at 276 nm. Moreover, a calibration curve (Fig. S1) was prepared by the same method in 10, 20, 30, 40, 50, and 60 mg/L of pre-defined BPA stock solutions. The degradation performance of BPS and BPAF in the triphase photocatalytic system for BPS and BPAF were tested by the same method.

3. Results and discussion

The concept is schematically shown in Fig. 1a. The triphase system was constructed by placing Au/TiO_2 immobilized GDL onto the top of the BPA solution phase. In this way, oxygen in the air can enter the gas-liquid-solid triphase interface through the porous GDL and then reacts with photo-excited carriers on Au/TiO_2 for ROS generation and BPA oxidation. The cross-sectional scanning electron microscope (SEM) image in Fig. 1b illustrated the configuration of the immobilized Au/TiO_2 on GDL. The thickness of photocatalyst Au/TiO_2 was estimated to be 1.0 ± 0.2 μm from the energy-dispersive X-ray spectroscopy mapping result of Ti and C elements in the selected region (Fig. 1c). The enlarged SEM image in Fig. 1d shows the top-view morphology of carbon nanoparticles on GDL, which possesses a water contact angle (CA) of 142° showing hydrophobic property. After immobilization of the Au/TiO_2 layer, the water CA sharply dropped to nearly 0° because of the superhydrophilic property of nanosized Au/TiO_2 shown in Fig. 1e. More structure details of the Au/TiO_2 photocatalysts layer were further investigated. As shown in the X-ray diffraction pattern (Fig. S2), the photocatalysts used in our study were composed of anatase and rutile TiO_2. Only a faint diffraction peak of Au was observed at about 38°, probably because of the low Au content [23]. The relative intensity of anatase and rutile phases was estimated to be 4/1, which was essentially equal to that found for the pristine TiO_2 support, thus leading to the conclusion that the structure of TiO_2 did not undergo significant changes throughout the synthetic processes. From TEM images (Fig. S3), high-angle annular dark-field scanning TEM (HAADF-STEM) image (Fig. 1f), and energy-dispersive X-ray spectroscopy element mapping (Fig. 1g), the size of isolated TiO_2 particles was about 30 nm, and the size of Au particles was around 5–10 nm. The size distribution of Au nanoparticles is shown in Fig. S4. The lattice spacing of 2.36 Å and 3.52 Å supports the (111) planes of Au and the (101) planes of anatase TiO_2, respectively. Diffuse reflection spectra of both pristine TiO_2 and Au/TiO_2 nanoparticles displayed in Fig. S5 revealed a strong light absorption in the UV light region. Hence, a 365 nm light source (Fig. S6) was used to evaluate photocatalytic BPA degradation efficiency. Moreover, we found that Au/TiO_2 can produce ROS with free radical capture experiments (Fig. S7).

First of all, carbon-based GDL and polytetrafluoroethylene GDL have similar catalytic performance (Fig. S8), indicating that the GDL substrate has little effect on photocatalytic performance. As shown in Fig. 2a, a degradation percentage of more than 60% was achieved over Au/TiO_2-based on the triphase system within 120 min UV irradiation at 40 mW/cm^2. While for a diphase system, where Au/TiO_2 was immobilized onto a quartz substrate immersed in the bulk liquid phase, BPA was approximately not degraded under the same conditions. Another diphase control system was performed by immersing Au/TiO_2 loaded GDL into the water phase and got a similar result (Fig. S9). It is hypothesized that the noticeable BPA degradation efficiency difference between triphase and diphase systems is mainly because of the interfacial oxygen diffusion-controlled charge separation and aerobic oxidation processes.

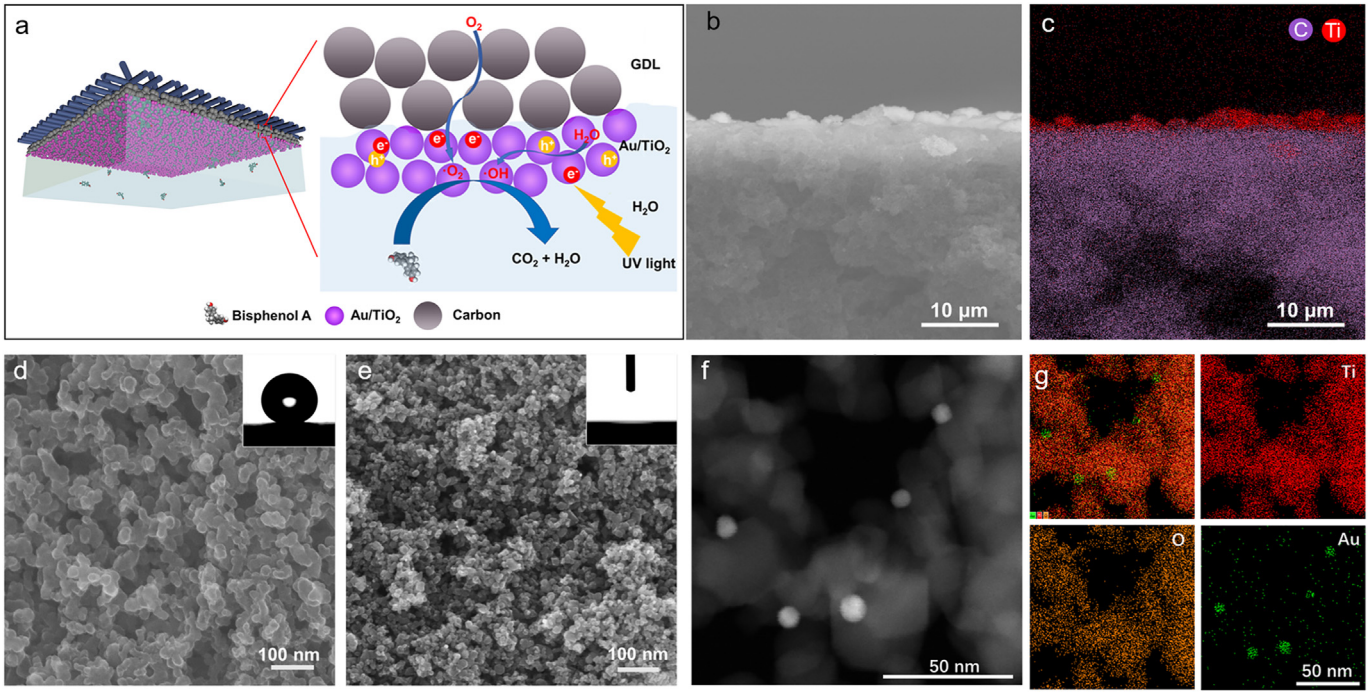

Fig. 1. Structural characterization of the Au/TiO_2-immobilized GDL. (**a**) Schematic illustration of the triphase photocatalytic system and enlarged view of the gas-liquid-solid triphase reaction interface. (**b**) Cross-sectional SEM image of Au/TiO_2-immobilized GDL. (**c**) Corresponding EDS mapping of Au/TiO_2-immobilized GDL. (**d**) Top-view SEM image of carbon black GDL. (**e**) Top-view SEM image of immobilized Au/TiO_2 layer. Inserts in (d) and (e) show photographs of water droplets on each sample. (**f**) HAADF-STEM image of Au/TiO_2. (**g**) EDS element maps for Ti, O, and Au. EDS, energy-dispersive X-ray spectroscopy; GDL, gas diffusion layer; SEM, scanning electron microscopy.

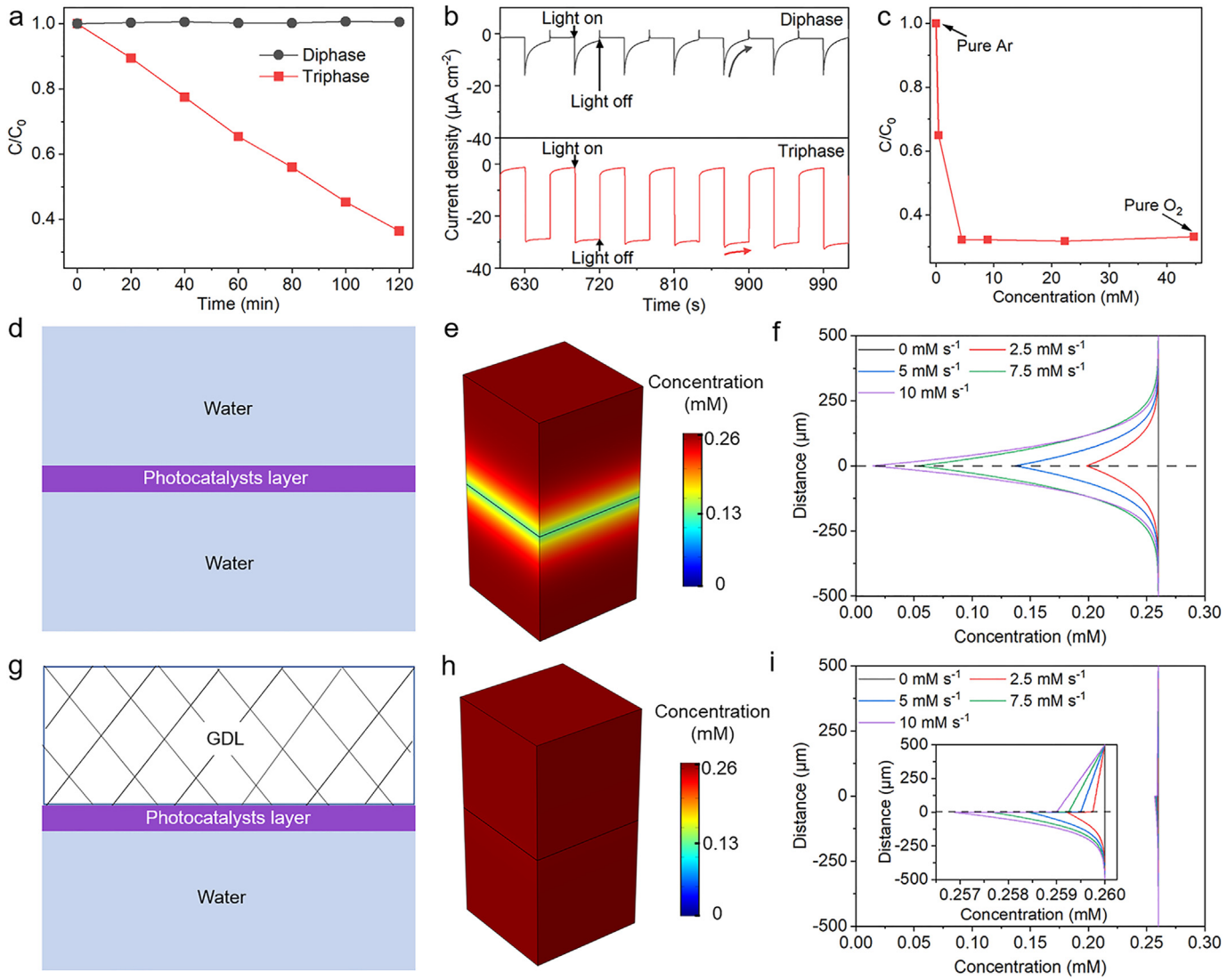

Fig. 2. (**a**) Photocatalytic aerobic oxidation of BPA in the triphase system and diphase system under the irradiation of UV light, light intensity = 40 mW/cm^2. (**b**) Photocurrent density comparison between triphase system and diphase system. (**c**) BPA degradation performance at different oxygen concentrations. (**d**) Schematic diagram of two phases immersed in the liquid phase. (**e**) Modeled oxygen diffusion in diphase system where the catalysts are immersed in liquid, oxygen consumption rate = 5 mM/s. (**f**) Corresponding oxygen concentration in the triphase system (data collected from (e)). (**g**) Schematic diagram of gas-liquid-solid triphase photocatalysis system. (**h**) Modeled oxygen diffusion in the triphase system where the catalysts are at the gas-liquid boundary, oxygen consumption rate = 5 mM/s. (**i**) Corresponding oxygen concentration in the triphase system (data collected from (h)). BPA, 2,2-bis(4-hydroxyphenyl)propane; UV, ultraviolet.

Therefore, diffusion-dependent photocurrent tests were first carried out. As illustrated in Fig. 2b, both the diphase and triphase systems show negligible dark currents. Negative photocurrent occurred under irradiation, indicating a photo-induced charge separation and oxygen reduction process over Au/TiO_2 photocathode. For the diphase system, the photocurrent intensity dramatically reduced from about 18 μA/cm^2 to near-zero within each 30 s chopped irradiation, indicating a severe oxygen diffusion-limited process owing to the slow oxygen mass transfer process in the liquid phase. On the contrary, the triphase system kept a photocurrent intensity at about 35 μA/cm^2 without obvious decay, suggesting a non-diffusion limited charge separation for oxygen photoactivation, which can be ascribed to the fast supply of oxygen molecules from the gas phase. Furthermore, by using gas sources with different O_2/Ar volume ratios, we found that the triphase system exhibited good tolerance to the gas-phase oxygen concentration for photocatalytic BPA oxidation and the removal of TOC (Figs. 2c and S10). Even for an oxygen concentration as low as 0.45 mM (1% volume fraction), the triphase system can maintain a BPA degradation percentage of more than 30%.

To analyze the influence of interfacial oxygen mass transfer and consumption on the local oxygen concentration of photocatalysts during photocatalysis, the local concentrations of O_2 in triphase and diphase systems were modeled in COMSOL 5.4 [24,25]. Three-dimensional geometric models (500 μm × 500 μm × 1000 μm) were built for the two systems (Fig. S11). For the diphase system, the model was composed of a photocatalysts layer with a thickness of 1 μm sandwiched in the middle of the water phase (schematically shown in Fig. 2d). For the triphase system, the same photocatalysts layer was sandwiched between the GDL and the water phase (schematically shown in Fig. 2g). A porous domain displayed in Fig. S12 with Bosanquet effective diffusivity was used for the GDL to calculate its effective diffusivity [26], which diminishes the effective gas diffusivity due to Knudsen diffusivity. An initial oxygen concentration of 0.26 mM was set for both systems according to the saturated oxygen solubility in the water phase. The oxygen

consumption rate region from 0 to 10 mM/s was estimated by the oxygen consumption rate for photodegradation of BPA in the triphase system (about 5 mM/s). As the simulated results are shown in Fig. 2e and f, the local oxygen concentration of the photocatalysts layer in the diphase system dramatically decreases as the oxygen consumption rate increases. On the contrary, the triphase system remains a high oxygen concentration in the local area of the photocatalysts layer, suggesting that the oxygen supply through the GDL is sufficient to meet the demand for oxygen consumption during the photocatalytic aerobic oxidation of BPA even in diluted conditions (Fig. 2h and i).

The effect of the initial concentration of BPA was further investigated and displayed in Fig. 3a. Au/TiO_2 showed 84%, 78%, 76%, 69%, and 64% degradation of BPA with 20, 30, 40, 50, and 60 mg/L initial concentration, respectively. This phenomenon revealed that the catalytic efficiency of the catalyst was decreased with increasing the initial concentration of BPA as a result of the shading effect for light [27]. The pseudo-first-order kinetic equation was used to describe the kinetics of the photocatalytic degradation of BPA. The degradation rate constants can be calculated by the following formula:

$$-ln\frac{C}{C_0} = kt$$

where k and t are the rate constant (min^{-1}) and reaction time (min), C and C_0 are BPA concentration at a specific moment and the initial concentration of BPA, respectively. As the initial concentration of BPA was increased, the rate constant was decreased (Fig. 2b) and found to be 0.0084 min^{-1} for an initial concentration of 60 mg/L (Table S1). Furthermore, the degradation of BPA accelerated significantly with the increase of light intensity. When the light intensity was increased from 5 mW/cm^2 to 200 mW/cm^2, the degradation percentage was increased from 20% to 85% (Fig. 3c), and the rate constant was also nearly increased tenfold from 0.0018 min^{-1} to 0.017 min^{-1} (Fig. 3d and Table S2). It is worth mentioning that the rate of photocatalytic aerobic oxidation for BPA degradation reached 0.425 mg/L/min, which is much higher than that reported in most literature under the same conditions [28–30].

For previous laboratory research on the photooxidation of pollutants, the stability evaluation of photocatalysts often requires the recycling of the photocatalytic nanomaterials from the water phase, which is cumbersome and difficult to achieve in practical applications. The construction of a continuous flowing photocatalytic system has the advantages of high operational safety, high production efficiency, and simple post-reaction processing and is especially suitable for potential large-scale industrial applications [31]. Consequently, the stability test of the triphase system was carried out in a homemade flow reactor. The flow reactor comprised of three components: aluminum alloy back frame with square through channels, serpentine water flow path, Au/TiO_2 immobilized GDL, and quartz window (Figs. 4a, b, and S13). The water flow rate was controlled by a peristaltic pump. Quartz window ensures that the UV light passes through the water layer to reach the surface of the photocatalysts. As shown in Fig. 4c, BPA can be degraded, and the reaction rate can be greatly improved by

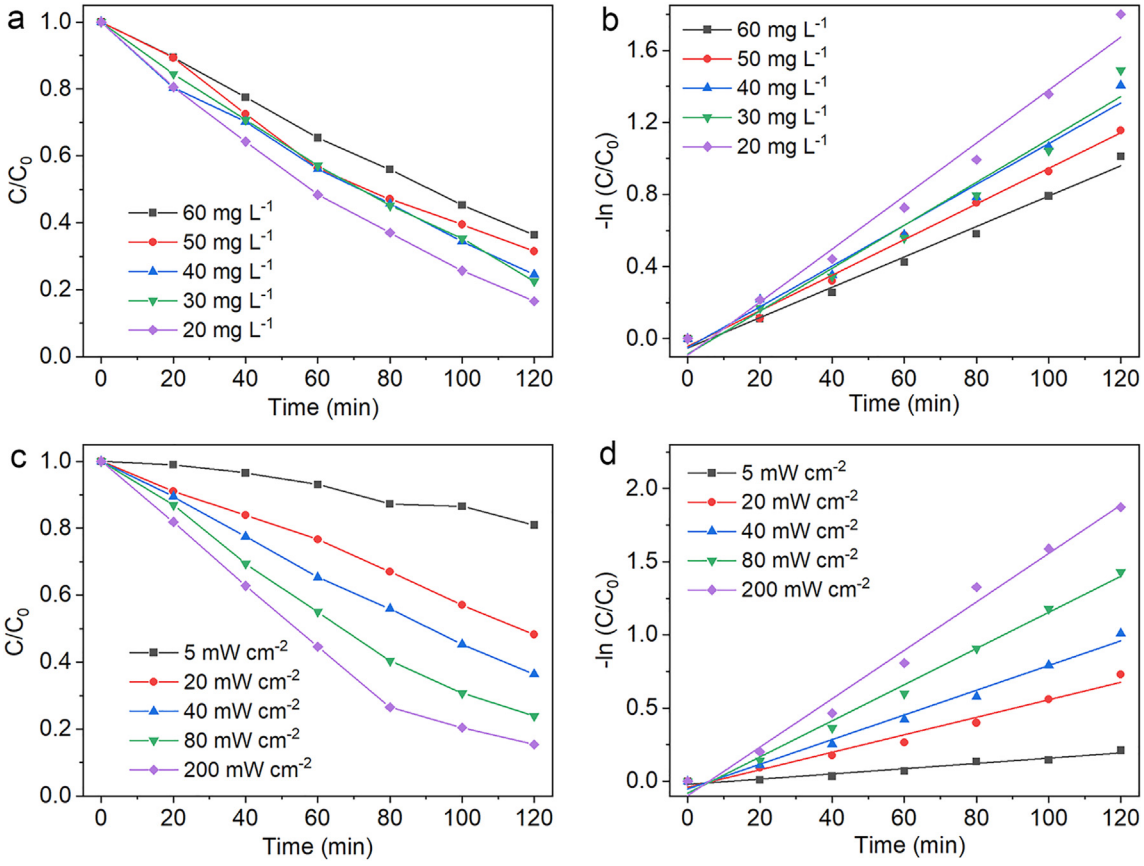

Fig. 3. (**a**) Photocatalytic aerobic oxidation for BPA degradation with different initial concentrations, light intensity = 40 mW/cm^2. (**b**) The pseudo-first-order fitting of (a). (**c**) BPA degradation activity under UV irradiation with different light intensities. (**d**) The pseudo-first-order fitting of (c). BPA, 2,2-bis(4-hydroxyphenyl)propane; UV, ultraviolet.

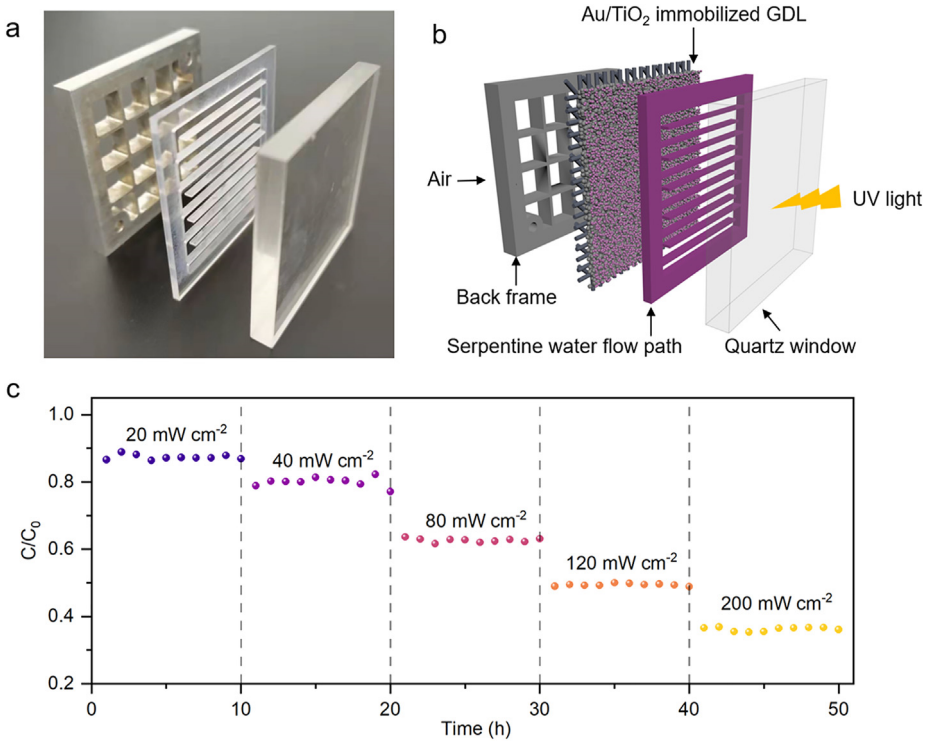

Fig. 4. (**a**) A photograph of the homemade triphase flow reactor. (**b**) Schematic illustration of the triphase flow photocatalytic system. (**c**) Time and UV intensity-dependent photocatalytic aerobic oxidation for BPA degradation based on the triphase flow reactor. UV, ultraviolet.

increasing the UV light intensity. As the light intensity gradually increased from 20 mW/cm^2 to 200 mW/cm^2, the degradation percentage of BPA increased from 10% to 60%. For better justification and understanding of the changes that may occur on catalyst structure, the SEM (Fig. S14) and XPS (Fig. S15) characterization of the catalyst after 50-h stability test was also carried out, showing that the structure and morphology of the catalyst and the GDL were not damaged, which may be the reason for its stable performance. The triphase photocatalytic organic pollutant degradation system also shows excellent removal performance for BPS and BPAF (Fig. S16).

4. Conclusion

In summary, we have constructed a gas-liquid-solid triphase photocatalytic system based on Au/TiO_2 nanoparticles to accomplish efficient photocatalytic aerobic oxidation for BPA degradation. This triphase system realized the rapid and continuous supply of reactant oxygen, thus promoting the charge separation and oxygen activation processes over photocatalysts for the effective photocatalytic aerobic oxidation of BPA. The interfacial oxygen mass transfer process during the reaction was analyzed through finite element simulation and diffusion-dependent photocurrent, which may become reliable guides for the research on the mass transfer issue for aerobic oxidation reactions. Furthermore, investigation on long-time operation stability for a flow triphase photocatalytic reactor demonstrates the bright prospects of this triphase system for the potential large-scale photocatalytic applications.

CRediT authorship contribution statement

Pu Wang: Methodology, Writing – original draft, Formal analysis, Software. **Jiaqi Zhao:** Methodology. **Run Shi:** Conceptualization, Writing – review & editing. **Xuerui Zhang:** Methodology. **Xiangdong Guo:** Software. **Qing Dai:** Supervision. **Tierui Zhang:** Funding acquisition, Project administration, Supervision.

Declaration of competing interest

The authors declare that they have no known competing financial interests or personal relationships that could have appeared to influence the work reported in this paper.

Acknowledgments

The authors are grateful for financial support from the National Key Projects for Fundamental Research and Development of China (2018YFB1502002), the National Natural Science Foundation of China (51825205, 52120105002, 51772305, 21902168), the Beijing Natural Science Foundation (2191002), the Strategic Priority Research Program of the Chinese Academy of Sciences (XDB17000000), the Royal Society-Newton Advanced Fellowship (NA170422), the International Partnership Program of Chinese Academy of Sciences (GJHZ201974) and the Youth Innovation Promotion Association of the CAS.

Appendix A. Supplementary data

Supplementary data to this article can be found online at https://doi.org/10.1016/j.mtener.2021.100908.

References

[1] G. Jiang, Preface to the special topic on environmental pollution and health risk, Natl. Sci. Rev. 3 (2016) 409-409, https://doi.org/10.1093/nsr/nww090.
[2] A. Shoneye, J. Tang, Highly dispersed FeOOH to enhance photocatalytic activity of TiO_2 for complete mineralisation of herbicides, Appl. Surf. Sci. 511 (2020) 145479, https://doi.org/10.1016/j.apsusc.2020.145479.

[3] J. Li, B. Zhou, Y. Liu, Q. Yang, W. Cai, Influence of the coexisting contaminants on bisphenol A sorption and desorption in soil, J. Hazard. Mater. 151 (2008) 389–393, https://doi.org/10.1016/j.jhazmat.2007.06.001.
[4] W. Guo, W. Hu, J. Pan, H. Zhou, W. Guan, X. Wang, J. Dai, L. Xu, Selective adsorption and separation of BPA from aqueous solution using novel molecularly imprinted polymers based on kaolinite/Fe_3O_4 composites, Chem. Eng. J. 171 (2011) 603–611, https://doi.org/10.1016/j.cej.2011.04.036.
[5] J.T. Grant, J.M. Venegas, W.P. McDermott, I. Hermans, Aerobic oxidations of light alkanes over solid metal oxide catalysts, Chem. Rev. 118 (2018) 2769–2815, https://doi.org/10.1021/acs.chemrev.7b00236.
[6] M. Ruokolainen, E. Ollikainen, T. Sikanen, T. Kotiaho, R. Kostiainen, Oxidation of tyrosine-phosphopeptides by titanium dioxide photocatalysis, J. Am. Chem. Soc. 138 (2016) 7452–7455, https://doi.org/10.1021/jacs.6b02472.
[7] J. Xu, T. Su, Z. Zhu, N. Chen, D. Hao, M. Wang, Y. Zhao, W. Ren, H. Lü, Biomimetic oxygen activation and electron transfer for aerobic oxidative 5-hydroxymethylfurfural to 2,5-diformylfuran, Chem. Eng. J. 396 (2020) 125303, https://doi.org/10.1016/j.cej.2020.125303.
[8] D. Ayodhya, G. Veerabhadram, A review on recent advances in photodegradation of dyes using doped and heterojunction based semiconductor metal sulfide nanostructures for environmental protection, Mater. Today Energy 9 (2018) 83–113, https://doi.org/10.1016/j.mtener.2018.05.007.
[9] J.G. Mahy, S.D. Lambert, R.G. Tilkin, C. Wolfs, D. Poelman, F. Devred, E.M. Gaigneaux, S. Douven, Ambient temperature ZrO_2-doped TiO_2 crystalline photocatalysts: highly efficient powders and films for water depollution, Mater. Today Energy 13 (2019) 312–322, https://doi.org/10.1016/j.mtener.2019.06.010.
[10] L. Ren, L. Tong, X. Yi, W. Zhou, D. Wang, L. Liu, J. Ye, Ultrathin graphene encapsulated Cu nanoparticles: a highly stable and efficient catalyst for photocatalytic H_2 evolution and degradation of isopropanol, Chem. Eng. J. 390 (2020) 124558, https://doi.org/10.1016/j.cej.2020.124558.
[11] Q. Guo, C. Zhou, Z. Ma, X. Yang, Fundamentals of TiO_2 photocatalysis: concepts, mechanisms, and challenges, Adv. Mater. 31 (2019) 1901997, https://doi.org/10.1002/adma.201901997.
[12] A. Meng, L. Zhang, B. Cheng, J. Yu, Dual cocatalysts in TiO_2 photocatalysis, Adv. Mater. 31 (2019) 1807660, https://doi.org/10.1002/adma.201807660.
[13] M. Teranishi, S.-i. Naya, H. Tada, In situ liquid phase synthesis of hydrogen peroxide from molecular oxygen using gold nanoparticle-loaded titanium(IV) dioxide photocatalyst, J. Am. Chem. Soc. 132 (2010) 7850–7851, https://doi.org/10.1021/ja102651g.
[14] S.N. Habisreutinger, L. Schmidt-Mende, J.K. Stolarczyk, Photocatalytic reduction of CO_2 on TiO_2 and other semiconductors, Angew. Chem. Int. Ed. 52 (2013) 7372–7408, https://doi.org/10.1002/anie.201207199.
[15] Z. Xu, W. Chai, J. Cao, F. Huang, T. Tong, S. Dong, Q. Qiao, L. Shi, H. Li, X. Qian, Z. Bian, Controlling the gas–water interface to enhance photocatalytic degradation of volatile organic compounds, ACS ES&T Eng. 1 (2021) 1140–1148, https://doi.org/10.1021/acsestengg.1c00120.
[16] J. Wang, J. Li, H. Li, S. Duan, S. Meng, X. Fu, S. Chen, Crystal phase-controlled synthesis of $BiPO_4$ and the effect of phase structure on the photocatalytic degradation of gaseous benzene, Chem. Eng. J. 330 (2017) 433–441, https://doi.org/10.1016/j.cej.2017.07.121.
[17] Z. Jiang, L. Wang, J. Lei, Y. Liu, J. Zhang, Photo-Fenton degradation of phenol by CdS/rGO/Fe^{2+} at natural pH with in situ-generated H_2O_2, Appl. Catal. B Environ. 241 (2019) 367–374, https://doi.org/10.1016/j.apcatb.2018.09.049.
[18] X. Sheng, Z. Liu, R. Zeng, L. Chen, X. Feng, L. Jiang, Enhanced photocatalytic reaction at air–liquid–solid joint interfaces, J. Am. Chem. Soc. 139 (2017) 12402–12405, https://doi.org/10.1021/jacs.7b07187.
[19] Z. Liu, X. Sheng, D. Wang, X. Feng, Efficient hydrogen peroxide generation utilizing photocatalytic oxygen reduction at a triphase interface, iScience 17 (2019) 67–73, https://doi.org/10.1016/j.isci.2019.06.023.
[20] R. Shi, J. Guo, X. Zhang, G.I.N. Waterhouse, Z. Han, Y. Zhao, L. Shang, C. Zhou, L. Jiang, T. Zhang, Efficient wettability-controlled electroreduction of CO_2 to CO at Au/C interfaces, Nat. Commun. 11 (2020) 3028, https://doi.org/10.1038/s41467-020-16847-9.
[21] Z. Cai, Y. Zhang, Y. Zhao, Y. Wu, W. Xu, X. Wen, Y. Zhong, Y. Zhang, W. Liu, H. Wang, Y. Kuang, X. Sun, Selectivity regulation of CO_2 electroreduction through contact interface engineering on superwetting Cu nanoarray electrodes, Nano Res. 12 (2019) 345–349, https://doi.org/10.1007/s12274-018-2221-7.
[22] L. Chen, X. Sheng, D. Wang, J. Liu, R. Sun, L. Jiang, X. Feng, High-performance triphase bio-photoelectrochemical assay system based on superhydrophobic substrate-supported TiO_2 nanowire arrays, Adv. Funct. Mater. 28 (2018) 1801483, https://doi.org/10.1002/adfm.201801483.
[23] A.V. Puga, A. Forneli, H. García, A. Corma, Production of H_2 by ethanol photoreforming on Au/TiO_2, Adv. Funct. Mater. 24 (2014) 241–248, https://doi.org/10.1002/adfm.201301907.
[24] P. Zhai, X. Gu, Y. Wei, J. Zuo, Q. Chen, W. Liu, H. Jiang, X. Wang, Y. Gong, Enhanced mass transfer in three-dimensional single-atom nickel catalyst with open-pore structure for highly efficient CO_2 electrolysis, J.Energy Chem. 62 (2021) 43–50, https://doi.org/10.1016/j.jechem.2021.03.011.
[25] F.P. García de Arquer, C.-T. Dinh, A. Ozden, J. Wicks, C. McCallum, R. Kirmani Ahmad, D.-H. Nam, C. Gabardo, A. Seifitokaldani, X. Wang, C. Li Yuguang, F. Li, J. Edwards, J. Richter Lee, J. Thorpe Steven, D. Sinton, H. Sargent Edward, CO_2 electrolysis to multicarbon products at activities greater than 1 A cm^{-2}, Science 367 (2020) 661–666, https://doi.org/10.1126/science.aay4217.
[26] D. Shou, J. Fan, M. Mei, F. Ding, An analytical model for gas diffusion though nanoscale and microscale fibrous media, Microfluid. Nanofluidics 16 (2014) 381–389, https://doi.org/10.1007/s10404-013-1215-8.
[27] T. Ahamad, M. Naushad, Y. Alzaharani, S.M. Alshehri, Photocatalytic degradation of bisphenol-A with g-C_3N_4/MoS_2-PANI nanocomposite: kinetics, main active species, intermediates and pathways, J. Mol. Liq. 311 (2020) 113339, https://doi.org/10.1016/j.molliq.2020.113339.
[28] S. Xiao, C. Zhou, X. Ye, Z. Lian, N. Zhang, J. Yang, W. Chen, H. Li, Solid-phase microwave reduction of WO_3 by GO for enhanced synergistic photo-fenton catalytic degradation of bisphenol A, ACS Appl. Mater. Interfaces 12 (2020) 32604–32614, https://doi.org/10.1021/acsami.0c06373.
[29] X. Liang, G. Wang, X. Dong, G. Wang, H. Ma, X. Zhang, Graphitic carbon nitride with carbon vacancies for photocatalytic degradation of bisphenol A, ACS Appl. Nano Mater. 2 (2019) 517–524, https://doi.org/10.1021/acsanm.8b02089.
[30] C. Zhang, W. Fei, H. Wang, N. Li, D. Chen, Q. Xu, H. Li, J. He, J. Lu, p-n Heterojunction of BiOI/ZnO nanorod arrays for piezo-photocatalytic degradation of bisphenol A in water, J. Hazard. Mater. 399 (2020) 123109, https://doi.org/10.1016/j.jhazmat.2020.123109.
[31] P. Ji, X. Feng, P. Oliveres, Z. Li, A. Murakami, C. Wang, W. Lin, Strongly Lewis acidic metal–organic frameworks for continuous flow catalysis, J. Am. Chem. Soc. 141 (2019) 14878–14888, https://doi.org/10.1021/jacs.9b07891.